

HIGH-RESOLUTION SPECTROSCOPY OF HIGHLY EXCITED ELECTRONIC STATES BY PULSED–cw DOUBLE RESONANCE IN A MOLECULAR BEAM. A STUDY OF THE NO(E–A) SYSTEM

Gerard MEIJER, Maarten EBBEN and J.J. TER MEULEN

*Department of Molecular and Laser Physics, Katholieke Universiteit Nijmegen,
Toernooiveld, 6525 ED Nijmegen, The Netherlands*

Received 11 July 1988

An experimental technique in which the high power of a pulsed laser is combined with the narrow bandwidth of a cw laser has been used to study the NO($E^2\Sigma^+$, $v=0 \leftarrow A^2\Sigma^+$, $v=0$) band under high resolution. The spin–rotation splitting in the $E^2\Sigma^+$, $v=0$ state is determined, and a value for the splitting constant γ of -3.15 ± 0.20 MHz is found. A small perturbation of the $E^2\Sigma^+$, $v=0$ state is observed and is explained by an interaction with the $B^2\Pi$, $v=17$ state. From time-resolved fluorescence measurements a lifetime of $\tau = 41 \pm 2$ ns is found for the $E^2\Sigma^+$, $v=0$ state. The coupling of the E state and the A state with the cw laser results in a time-resolved $E \rightarrow A$ fluorescence curve which must be described using the optical Bloch equations. Rabi oscillations seen in the experimental curves can be correctly simulated using this quantum-mechanical description.

1. Introduction

In the last two decades several laser spectroscopic methods have been developed to study highly excited electronic states of atoms and molecules [1]. With the rapid progress of pulsed laser technology intense radiation ranging far into the ultraviolet has become available [2]. Multiphoton processes or double-resonance techniques using several pulsed lasers are successfully applied to reach the special electronic states one wants to investigate. These may be states that are energetically difficult to reach with one single photon [3], or states that are forbidden in electric dipole one-photon transitions [4]. The detection scheme used in these experiments depends on the dynamical properties of the excited state molecules and is based, for example, on fluorescence detection or detection of fluorescence dips, ion detection [5] or photofragment detection [6]. The ultimate spectral resolution in these experiments is often determined by the bandwidth of the laser system used, although in many cases other broadening mechanisms, especially lifetime broadening, may

be the limiting factor. With a typical bandwidth of pulsed laser systems of 0.01 cm^{-1} or larger, this means the finer structures of the electronic states are not observable. Although cw injection locked pulsed lasers can reach a bandwidth about a factor of 4 smaller than the value quoted above [7], this bandwidth is still orders of magnitude larger than that obtainable with single mode cw lasers.

In combination with molecular beam techniques or other Doppler-width reducing or Doppler-free methods, single-mode cw lasers allow a spectral resolution of several MHz [8]. High-resolution studies of this kind have been performed in the visible and near UV on both stable molecules and transient species [9]. A disadvantage of cw lasers, however, is the difficulty of reaching the far UV. Only in favorable cases is it possible to induce two-photon transitions to highly excited states with tightly focused intense cw laser beams [10,11].

In this paper we present a double-resonance technique in which full advantage of the specific properties of a pulsed laser and a cw laser is taken; the pulsed laser is used to reach high-en-

ergy states whereas the cw laser is used for its resolving power. Some preliminary results were already presented in a recent letter [12]. A similar technique has been applied in experiments in which autoionization of Rydberg levels of NO and H_2 is studied [13].

We investigated the NO molecule in a well-defined collimated molecular beam. The excitation scheme we used is indicated in fig. 1. Pulsed laser radiation around 226 nm is used to reach the first electronically excited $A^2\Sigma^+$, $v' = 0$ state of NO. Population of single rotational levels, monitored by the laser induced $A \rightarrow X$ fluorescence is possible. From the $A^2\Sigma^+$, $v' = 0$ state the NO molecules are excited with single frequency 600 nm cw radiation to the $E^2\Sigma^+$, $v' = 0$ state. Both electronically excited states are studied under high resolution by detecting the resonant $E \rightarrow A$ fluorescence. The spectral resolution we obtained is mainly determined by the residual Doppler broadening due to the divergence of the molecular beam and is about 17 MHz. This resolution allows the spin-rotation splitting constant γ of the $E^2\Sigma^+$, $v' = 0$ state to be determined. An effect of a heterogeneous perturbation between the $E^2\Sigma^+$,

$v' = 0$ and the $B^2\Pi$, $v' = 17$ states is observed and analyzed. This perturbation had not been observed in previous [14] Doppler limited spectroscopic studies. Time-resolved fluorescence from the excited states gives information on the magnitude of the radiative loss channels out of these states. The time-resolved fluorescence from the E state allows the experimental study of a (more or less) isolated two-level system, with coherent pumping and with radiative losses out of both levels. The time dependence of this fluorescence could be correctly described using the optical Bloch equations.

General applications of this double-resonance technique as well as possible experimental improvements are discussed.

2. Description of the apparatus

The pulsed laser system consists of a Lambda Physik dye laser with one amplifier stage operating on coumarin 47 dye, pumped with an XeF (351 nm) excimer laser. The typical dye laser output of 10 mJ in a 10 ns pulse was frequency doubled in an angle tunable β -BaB₂O₂ (BBO) crystal [15], made in the People's Republic of China and supplied by GWU, Germany. Our crystal was cut at an angle of 65°, the phase matching angle for doubling of 440 nm radiation, and had to be rotated 7° to produce the desired 226 nm. As the acceptance angle of this crystal is quite small [16], a laser beam as parallel as possible was coupled into the crystal. With an impressive efficiency of nearly 30% several mJ of tunable UV radiation were easily produced in this way. As no etalon was used inside the dye laser cavity the bandwidth of the UV radiation was about 0.5 cm^{-1} . Although this is orders of magnitude larger than the absorption linewidth of the NO molecules in the beam, we did not try to reduce this bandwidth any further. Even now, without focusing the UV radiation, we could saturate the NO $E^2\Sigma^+$, $v' = 0 \leftarrow A^2\Sigma^+$, $v'' = 0$ transition, as could be inferred from the LIF measurements. Furthermore it was much easier to keep the pulsed laser fixed on a certain rotational transition, and to populate different fine-structure levels of the

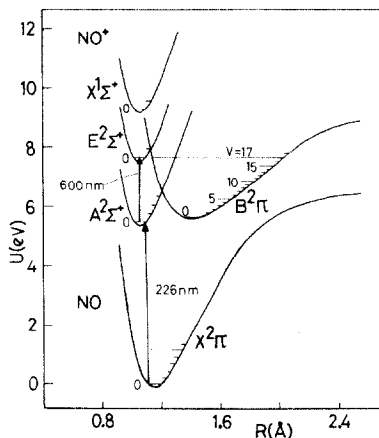


Fig. 1. Selected potential energy curves of NO (after ref. [33]) and schematic representation of the excitation process we used. Pulsed laser radiation around 226 nm is used to induce the $A \leftarrow X$ transition, and in the next step cw laser radiation around 600 nm pumps the excited molecules further up to the E state. The $B^2\Pi$, $v = 17$ state lies at almost the same energy as the $E^2\Sigma^+$, $v = 0$ state and a small effect of the perturbation between these states is seen in the $E \leftarrow A$ spectra.

$A^2\Sigma^+$, $v' = 0$ state simultaneously. The importance of this latter fact will be clarified in the discussion of the measurements of the spin-rotation doubling in the $E^2\Sigma^+$ state. The pulsed laser system operated most times at a repetition rate of 15 Hz.

The cw laser radiation was produced by a ring dye laser (Spectra Physics) operating on rhodamine 6G and pumped with 5 W of an Ar-ion laser. Relatively low output powers between 0.5 and 60 mW were used for the experiment. The bandwidth of this laser system, determined by the high-frequency jitter, is less than 0.3 MHz. Single-mode laser scans over a spectral range of about 40 GHz could be made.

To ensure high resolution the double-resonance experiment was performed on a well-defined beam of NO molecules. The NO gas was expanded through a 150 μm diameter nozzle into a chamber pumped with two 70 ℓ/s Roots pumps at a typical pressure of 0.05 mbar. The backing gas pressures of NO were varied between 400 and 700 mbar. A conical skimmer of 1.3 mm formed the molecular beam. The beam passed through two differentially pumped vacuum chambers and was collimated further by an adjustable diaphragm. In the detection region, about 15 cm downstream of the beam orifice, the background pressure was below 10^{-5} mbar, to ensure collision free conditions. Here the counter-propagating pulsed UV laser beam and the cw red laser beam cross the molecular beam perpendicularly. Both laser beams were unfocused and have a more or less circular intersection with the molecular beam of typically 2.0 mm for the cw laser beam and a somewhat smaller value of 1.0 mm for the pulsed laser beam. The polarization of both lasers was in the same plane, although this turned out to be unimportant even at low laser powers (far from saturation); no effects of anisotropy of the double-resonance fluorescence were observed when the polarization of one laser was rotated with respect to the polarization of the other. The laser induced fluorescence was collected at right angles to both the molecular beam and the laser beams and imaged on the entrance window of the photomultiplier (EMI 9863 B). This PMT has a quantum efficiency of about 25% in the 200–300 nm region whereas the quantum ef-

iciency for radiation of around 600 nm is roughly a factor of three less. The fluorescence signal thus obtained was fed into a boxcar integrator and simultaneously displayed on a digital oscilloscope. With an appropriate setting of the gate of the boxcar the total fluorescence, averaged over 10 or 30 samples, was measured and recorded on a strip chart recorder. Time-resolved fluorescence curves were directly plotted from the oscilloscope.

In the double-resonance experiment the pulsed laser was usually kept fixed in frequency to populate a certain rotational level N' in the $A^2\Sigma^+$, $v' = 0$ state. This first step was controlled by looking for the resulting $A \rightarrow X$ fluorescence. Once this laser was set at the correct frequency a cut-off filter transmitting essentially only radiation above 590 nm was inserted in front of the PMT, to block the UV background. The cw laser was then scanned and the resulting resonant $E \rightarrow A$ fluorescence, which is only a fraction of the total emission of the $E^2\Sigma^+$, $v' = 0$ state, could be measured against a zero background level. The only radiation background was due to scattered cw laser light, which was almost completely eliminated by the use of a narrow boxcar gate. The absolute frequency of the cw laser, used to induce a certain rotational transition in the $E \leftarrow A$ band [14], was determined by the simultaneous recording of the well cataloged I_2 absorption spectrum in a cell [17]. Linewidths and splittings between closely spaced lines were measured in terms of the distance between neighbouring transmission peaks of two interferometers. These temperature and pressure stabilized interferometers have a FSR of 298.81 ± 0.04 and 74.2 ± 0.1 MHz, respectively, and allow splittings between different lines, recorded in a single-mode laser scan, to be determined with an accuracy of several MHz.

3. The method

In this section some special features of the double-resonance technique we applied will be discussed and compared with double-resonance experiments in which only lasers of one type, pulsed or cw, are involved.

One of the first concerns in any combination of a pulsed laser and a cw laser is the large loss in

duty cycle. It should be explicitly noted, however, that this loss is not as large as the ratio of the duration of a laser pulse to its repetition time. It depends on the experimental setup as well as on certain properties of the molecular system under study. In the molecular beam machine the NO molecules travel with a speed of about 500 m/s and are irradiated with the pulsed laser over a length of 1 mm. With a repetition rate of 15 Hz this means that a fraction 3.0×10^{-5} of the beam is irradiated. With the high energy per pulse this fraction is excited very efficiently; in NO we nearly saturated the A ← X step. Another important factor is the bandwidth of the pulsed laser. This bandwidth is very large compared with the residual Doppler width in a molecular beam, so all velocity groups are excited equally well.

For the second step to be successfully applied the lifetime of the intermediate electronic state should not be too short. The lifetime of NO ($A^2\Sigma^+$, $v' = 0$) is known to be about 200 ns [18]. During this lifetime the excited molecules can absorb another photon. As the double resonance signal appears essentially in this period of time, the use of a boxcar with a gate width of 500 ns enables us to suppress both the scattered cw radiation and the dark current of the PMT. Due to the narrow bandwidth of the cw laser only a certain velocity group of excited molecules is selected to be promoted to the next electronic state.

If the first step were possible with a cw laser there would be no loss in duty cycle. On the other hand, the excitation to the A state would be less efficient. Moreover, both cw lasers must excite the same velocity group, which would make the spectral resolution even higher but the experiment more difficult. Another very important difference, however, is that in this latter case the double-resonance signal would be uniformly distributed in time. This means that stray laser light can give quite a large background.

In some particular cases the use of two cw lasers could be advantageous. However, our setup with an efficient excitation of the first step and with the possibility of time-resolved detection has a more general applicability and the large loss in duty cycle can be largely compensated for.

The application of two pulsed lasers is not a

good alternative when one desires high spectral resolution. With two pulsed lasers, however, the lifetime of the excited $E^2\Sigma^+$, $v' = 0$ state can be determined directly, without the need to deconvolve the time-resolved fluorescence curves. For this special purpose we used a second pulsed dye laser, pumped by a Nd:YAG laser and operating on R6G, with 1 mJ in a 6 ns pulse.

4. Spectroscopic investigation of the NO(E ← A) bands

4.1. Theory

The rotational, fine and hyperfine structure of NO in both $^2\Sigma^+$ states can be described by the effective Hamiltonian:

$$H = BN^2 - DN^4 + \gamma N \cdot S + bI \cdot S + cI_x S_x, \quad (1)$$

where N is the angular momentum vector of the end-over-end rotation of the molecule, S is the total electronic spin vector and I is the spin of the nitrogen nucleus. The values for the rotational constant B as well as for the centrifugal distortion D for both $^2\Sigma^+$ states are taken from the work of Amiot and Verges [14]. They analyzed the rotational structure of electronic emission bands involving these states in the near IR, using Fourier transform spectroscopy. An accurate value for the band origin ν_{00} of the $E^2\Sigma^+$, $v = 0 \leftarrow A^2\Sigma^+$, $v = 0$ electronic transition was also given in their work. The spin-rotation interaction $\gamma N \cdot S$ splits each N level by an amount $\gamma(N + 1/2)$ into two J levels, where $J = N + S$. For the NO($A^2\Sigma^+$, $v = 0$) state the magnitude of this γ constant is well known from a Doppler-free two-photon spectroscopic study of the NO(A ← X) transition, using a cw ring dye laser, as $\gamma = -80.35 \pm 0.15$ MHz [10]. A negative value for this constant γ means that F_1 levels ($J = N + 1/2$) are lower in energy than F_2 levels ($J = N - 1/2$). The ρ -doubling in the $E^2\Sigma^+$, $v = 0$ state was too small to be determined from the Doppler-limited Fourier transform spectra, and was therefore not known until now. We determined a value of $\gamma = -3.15 \pm 0.20$ MHz for this splitting which means the E state also has an

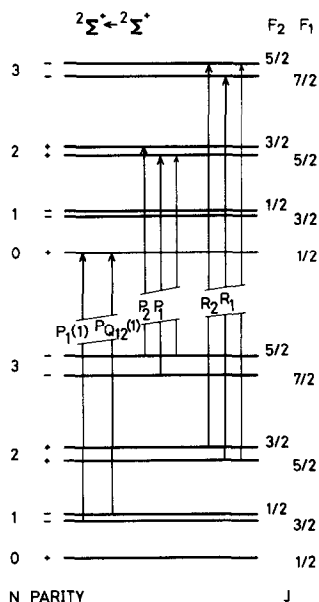


Fig. 2. Energy level scheme of both $2\Sigma^+$ states of NO. The inverted spin splitting, shown enlarged in the figure, gives F_2 levels that are higher in energy than the F_1 levels. In the left side of the figure the two possible transitions to the $N = 0$ level in the upper $2\Sigma^+$ state are indicated (see fig. 4). Except for the lowest rotational levels, pairs of lines from each ρ -doublet are seen. The weaker $\Delta J = 0$ transitions (thinner arrows) are not observed in this case. Two lines belonging to the same pair (e.g. $P_1(N)$ and $P_2(N)$) are separated by the difference in ρ -doubling in the upper and the lower state.

inverted fine structure. In fig. 2 the energy level structure for both $2\Sigma^+$ states is schematically presented.

For electric dipole transitions the $+\leftrightarrow-$ parity selection rule together with the $\Delta J = 0, \pm 1$ selection rule restricts the possible rotational transitions to $\Delta N = \pm 1$. There are six possible rotational branches, three starting from each fine structure level. The two $\Delta J = 0$ branches are very weak as they must change spin states, and can in practice only be observed for the lowest rotational levels. This means for higher energy levels only two pairs of closely spaced lines will show up in the spectrum. The splitting between the two almost equally strong lines belonging to the same ΔJ pair (between $P_1(N)$ and $P_2(N)$ or between $R_1(N)$ and $R_2(N)$) is equal to the difference in ρ doubling of the A state and the E state, as seen in the figure.

In both electronically excited states the hyperfine interaction due to the spin $I = 1$ of the nitrogen nucleus, splits each fine structure level into levels characterized by the total quantum number $F = J + I$. In the A state the hyperfine structure is well known for $v = 3$ [19]. We assume that the hyperfine structure in the $A^2\Sigma^+$, $v = 0$ level can be described using similar values for the Frosch and Foley parameters of $b \approx 40$ MHz and $c \approx 2$ MHz. The interaction between the electronic spin and the quadrupole moment of the nitrogen nucleus can be neglected within the present experimental accuracy.

4.2. General results

In fig. 3 two spectra are shown to demonstrate the double-resonance technique. The upper part of the figure shows a part of the normal LIF spectrum of the $\text{NO}(A^2\Sigma^+, v' = 0 \leftarrow X^2\Pi, v'' = 0)$

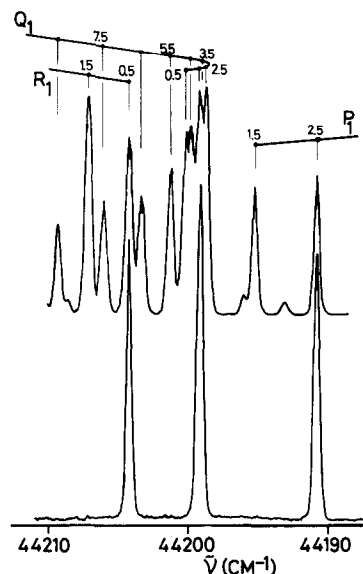


Fig. 3. Upper trace: Normal LIF spectrum of the $A \leftarrow X$ transition, induced by the pulsed laser. Lower trace: Double-resonance $E \rightarrow A$ fluorescence with the cw laser fixed on the $E \leftarrow A$ $P_1(1)$ transition, whereas the pulsed laser is scanned. Only transitions that reach the labeled hyperfine level in the A state are seen in double resonance. In both spectra the linewidth is determined by the bandwidth of the pulsed laser. The UV fluorescence (upper trace) is roughly a factor 100 more intense than the red fluorescence (lower trace).

transition, obtained by scanning the pulsed laser and detecting the total A \rightarrow X fluorescence. The cw laser is switched off here. The different rotational transitions induced are indicated by the J quantum number in the electronic ground state. In the lower part of the figure the double-resonance spectrum is shown. Now the cw laser is switched on and kept fixed on the $F' = 3/2 \leftarrow F'' = 5/2$ hyperfine component of the E $^2\Sigma^+$, $v = 0 \leftarrow A^2\Sigma^+$, $v = 0$ P₁(1) transition. Only the red E \rightarrow A fluorescence is now detected while the pulsed laser is scanned over the same part of the A \leftarrow X transition. Thus only transitions which reach the labeled $N = 1, J = 3/2, F = 5/2$ level in the A $^2\Sigma^+$, $v' = 0$ state are seen.

In both spectra the linewidth is determined by the bandwidth of the pulsed laser. Although these spectra are measured in a molecular beam, similar spectra could have been obtained in a cell, with a somewhat modified relative line intensity. In measurements where the pulsed laser was kept fixed on a certain transition while the cw laser was scanned, use of the molecular beam is necessary to reduce the linewidth. A typical high-resolution

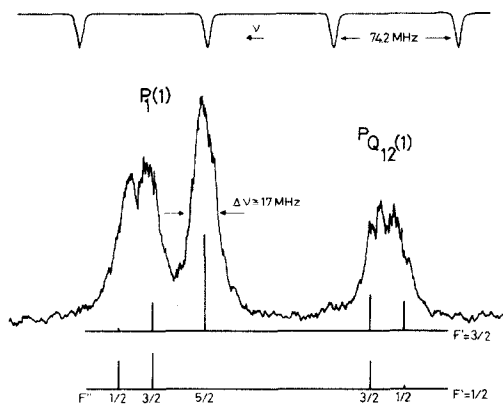


Fig. 4. High-resolution spectrum of the E \leftarrow A P₁(1) and P₁₂(1) transitions (see fig. 2). The pulsed laser is kept fixed in frequency. The hyperfine structure in the A $^2\Sigma^+$ state is shown partly resolved. The linewidth of 17 MHz for the single resolved hyperfine component is mainly determined by the residual Doppler broadening due to the divergence of the molecular beam.

E \leftarrow A spectrum of this latter type is shown in fig. 4. The pulsed laser is kept fixed in frequency and simultaneously excites on the A \leftarrow X Q₁(1) and the $^{\text{Q}}\text{P}_{21}$ (1) rotational transitions. Both fine structure levels of the A $^2\Sigma^+$, $v' = 0, N' = 1$ state are therefore populated. When the cw laser is scanned both the P₁(1) and the $^{\text{P}}\text{Q}_{12}$ (1) transitions of the E \leftarrow A band appear in the double-resonance spectrum. The line strength for these two transitions is the same which means the intensity of these lines in the spectrum directly reflects the degree of population of both fine structure levels in the A state by the pulsed laser. From this it can be concluded that the pulsed laser is not saturating the first step, as the expected intensity ratio of 3:1 is almost observed. The signal-to-noise ratio in this double-resonance spectrum is quite low, mainly because the adjustable diaphragm of the molecular beam was only opened 0.3 mm, to ensure narrow lines. Furthermore the power of the cw laser is only 4 mW to avoid power broadening effects. The linewidth of 17 MHz was the minimum linewidth obtainable, and is mainly determined by residual Doppler broadening due to the divergence of the molecular beam. As will be shown later the contribution to the linewidth caused by the finite lifetime of both electronically excited states is only of the order of 5 MHz. In almost all other measurements the diaphragm was opened up to 3 mm and a higher cw laser power was used. This increased the linewidth only to 25 MHz (fwhm) and a SNR of 1000 or better was achieved on the lowest rotational transitions, by averaging over 30 samples (2 s).

In the P₁(1) transition the hyperfine structure due to the splitting in the A $^2\Sigma^+$ state can be clearly recognized. The vertical bars underneath the experimental curve indicate the positions and intensities of the individual hyperfine components. The horizontal bars contain transitions to either one of the two possible F' levels in the E state. Their relative position is determined by the splitting between both F' levels. Positioning these bars exactly underneath each other means no hyperfine splitting in the E state is assumed. From this and similar spectra an upper limit for the Fermi contact term $b_{\text{F}} = b + c/3$ in the E state of $b_{\text{F}} \leq 15$ MHz can be given.

4.3. ρ -doubling in $E^2\Sigma^+$, $v' = 0$

A quite extensive series of measurements has been performed to determine the magnitude of the spin-rotation splitting in the $E^2\Sigma^+$, $v' = 0$ state. As discussed in section 4.1 and shown in fig. 2 this ρ -doubling can be determined from an accurate measurement of the splitting between a $P_1(N)$ and a $P_2(N)$ or between a $R_1(N)$ and a $R_2(N)$ line. Such splittings were measured in single-mode laser scans. To make these measurements possible both fine structure levels for a given quantum number N in the $A^2\Sigma^+$, $v' = 0$ state must be populated. We chose to do this by pumping with the pulsed laser in the $A \leftarrow X$ R_1 and ${}^R Q_{21}$ branches. Both branches have equal line strengths and are induced simultaneously within the bandwidth of the laser. The satellite branch of the Q_1 branch is relatively weak, and makes excitation with the pulsed laser in the Q_1 and ${}^Q P_{21}$ branches less favorable. With the pulsed laser fixed on a certain $R_1(N)$ line, the cw laser was scanned to determine the splitting between lines from both fine structure levels in the $A^2\Sigma^+$, $v' = 0$, $N + 1$ state. Only measurements up to $N' = 17$ in the $E^2\Sigma^+$ state were possible because rotational levels with higher quantum numbers are less well populated in the molecular beam. Moreover, a Doppler broadened background double-resonance signal from the rotationally warmer background gas in the vacuum machine (at a pressure $\leq 10^{-5}$ mbar) becomes relatively more important for higher levels.

In table 1 the observed splittings between different rotational transitions are given. Each value is the averaged result from at least six laser scans. The error given is one standard deviation. The splittings are measured between the centers of the more or less Gaussian envelopes of the rotational transitions, consisting of several unresolved hyperfine components. The hyperfine transitions with $\Delta F \neq \Delta J$ are weaker by a factor of J^2 than the $\Delta F = \Delta J$ transitions, which means only three hyperfine transitions will contribute for high J . As the position of the different hyperfine levels is not symmetrically distributed around the position of the unsplit fine structure level, this has to be corrected for. When only the Fermi contact interaction in the A state is considered as being re-

Table 1

Observed splittings (MHz) of rotational transitions in the $E^2\Sigma^+$, $v = 0 \leftarrow A^2\Sigma^+$, $v = 0$ band due to spin-rotation interaction in both coupled electronic states. The error given is equal to one standard deviation in the average of at least six measurements

Transition	Observed splitting (MHz)
$P_1(5)$ – $P_2(5)$	431.0 ± 3.0
$P_1(9)$ – $P_2(9)$	738.9 ± 3.0
$R_1(8)$ – $R_2(8)$	656.9 ± 3.0
$R_1(9)$ – $R_2(9)$	733.0 ± 3.0
$P_1(12)$ – $P_2(12)$	970.8 ± 3.5
$R_1(11)$ – $R_2(11)$	888.7 ± 6.0
$R_1(12)$ – $R_2(12)$	973.9 ± 3.0
$P_1(14)$ – $P_2(14)$	1132.7 ± 3.0
$R_1(13)$ – $R_2(13)$	1018.0 ± 4.5
$P_1(15)$ – $P_2(15)$	1178.5 ± 3.5
$R_1(14)$ – $R_2(14)$	1142.8 ± 3.5
$R_1(15)$ – $R_2(15)$	1183.8 ± 6.0
$R_1(16)$ – $R_2(16)$	1281.2 ± 6.0

sponsible for the hyperfine structure, it can be shown that the observed splittings as given in table 1 have to be reduced by an amount $4b/(6N + 3)$ to obtain the real difference in ρ -doubling between the two states. This correction is in most cases far within the experimental error. The selection of the R_1 branch to populate A state levels does not introduce any systematic error, as all hyperfine levels are nearly equally populated. For some transitions this has been checked experimentally by excitation with the pulsed laser in the Q_1 branch as well.

In fig. 5 the ρ -doubling in the $E^2\Sigma^+$, $v' = 0$ state is given as a function of the rotational quantum number N . These values are obtained from the data presented in table 1 after correcting for the ρ -doubling in the A state as well as for the minor effect of the hyperfine splitting in the A state, as discussed above. For low rotational quantum numbers the spin-rotation splitting increases linearly with N , as expected, but in the region $N = 13$ to $N = 17$ the effect of a perturbation is seen. The small size of this perturbation explains why it escaped prior observation, and explicitly demonstrates the high resolution obtainable with the present technique. This perturbation is due to the $v = 17$ level of the $B^2\Pi$ state

which nearly coincides with the $E^2\Sigma^+$, $v'=0$ state in this region, as shown in fig. 6. Unfortunately, spectroscopic information on the $v=17$ level of the $B^2\Pi$ state is scarce; in VUV absorption studies transitions to this vibrational level are hidden under the $B'^2\Delta$, $v'=1 \leftarrow X^2\Pi$, $v''=0$ band and, of course, under the $E^2\Sigma^+$, $v'=0 \leftarrow X^2\Pi$, $v''=0$ band. Only a few rotational transitions of the $B^2\Pi_{1/2}$, $v'=17 \leftarrow X^2\Pi_{1/2}$, $v''=0$ band up to $N'=11$ in the upper state are given in the literature [20]. Using these transition frequencies and taking the known term values in the electronic ground state [21], we fitted the rotational structure of the $B^2\Pi$, $v'=17$ state, and extrapolated to higher rotational levels. Neither centrifugal distortion nor Λ -doubling corrections were included. As only transitions to the $B^2\Pi_{1/2}$ spin multiplet are tabulated [20] the spin-orbit interaction constant A could not be fitted. A value of $A = 58 \text{ cm}^{-1}$ was taken as an interpolation between the (deperturbed) spin-orbit splitting constants of neighbouring vibrational levels [22]. The accuracy of the thus obtained rotational energies of the B state is estimated to be about 1 cm^{-1} .

It should be noted that the $E^2\Sigma^+$ state is a $4s\sigma$ Rydberg state, differing in two electron orbitals

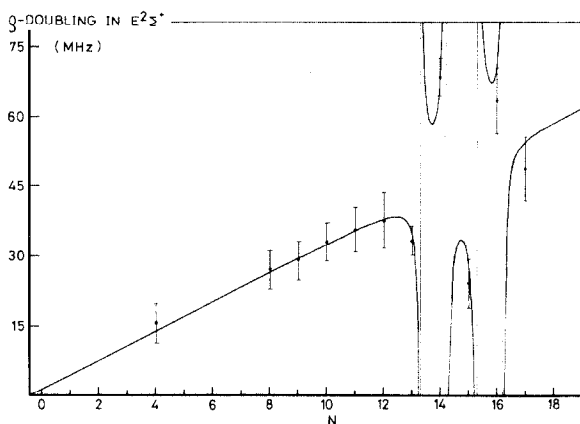


Fig. 5. Magnitude of the observed ρ -doubling in the $E^2\Sigma^+$, $v'=0$ state as a function of the rotational quantum number N . The best fit to the experimental points, which includes the effect of the perturbation between the $E^2\Sigma^+$ state and the $B^2\Pi$ state, is also given.

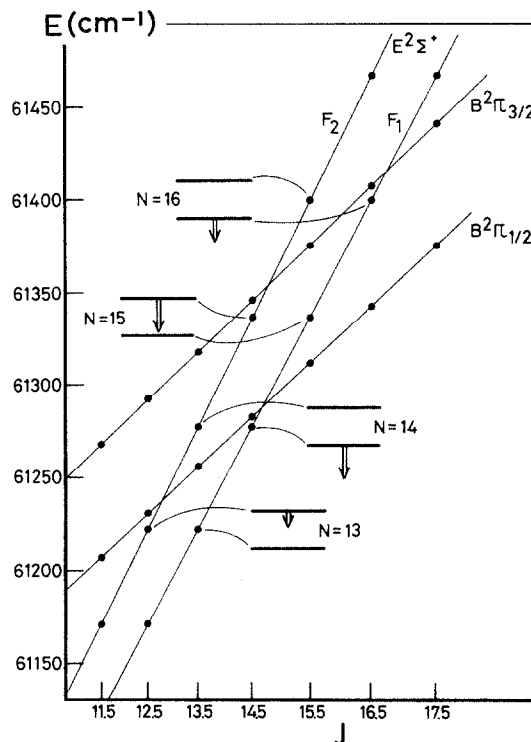


Fig. 6. Total energy curves of the $E^2\Sigma^+$, $v'=0$ and the $B^2\Pi$, $v=17$ states. The crossing between $J=12.5$ and $J=16.5$ causes the observed perturbations. In the figure only the effect of the strongest interactions (i.e. interactions with those levels of the same J that are closest) are taken into account to explain quantitatively the deviations from a linear N dependence, as observed in fig. 5.

from the $\pi^3\pi^2$ $B^2\Pi$ valence state. Therefore, a coupling between these states via one-electron operators is not possible and formally, a perturbation between these states is configurationally forbidden. Only when configuration interaction and/or two electron operators are taken into account such a perturbation can be explained [23].

In fig. 6 we have schematically indicated how the magnitude of the ρ -doubling in the E state is affected in the neighbourhood of a crossing. Although only the strongest interactions are taken into account in this simplified picture, it qualitatively explains the deviations observed in fig. 5. In a more quantitative description the shift of the energy level E_i due to the interaction with levels of the same symmetry and with the same quantum

number J positioned at an energy E_k is proportional to

$$\sum_k \frac{H_{ik}^2}{E_i - E_k}. \quad (2)$$

This approximation is correct as long as $H_{ik} \ll |E_i - E_k|$, thus when the total shift of the energy levels is small compared with their unperturbed energy distance. In our case this approximation is certainly correct. The matrix element H_{ik} for a ${}^2\Sigma^+ - {}^2\Pi$ (Hund's case (a)) interaction is given by Kovacs [24] as:

$$\begin{aligned} \langle {}^2\Sigma^+, J, N = J \pm 1/2 | H | {}^2\Pi_{3/2}, J \rangle \\ = -2\eta[(J - 1/2)(J + 3/2)]^{1/2}, \\ \langle {}^2\Sigma^+, J, N = J - 1/2 | H | {}^2\Pi_{1/2}, J \rangle \\ = \xi - 2\eta(J - 1/2), \\ \langle {}^2\Sigma^+, J, N = J + 1/2 | H | {}^2\Pi_{1/2}, J \rangle \\ = \xi + 2\eta(J + 3/2). \end{aligned} \quad (3)$$

In a least-squares fit program the observed ρ -doubling in the $E^2\Sigma^+$ state shown in fig. 5 is fit to an expression including both the expected $\gamma_E(N + 1/2)$ dependence and the interaction with the $B^2\Pi$ state. For each J level in the $B^2\Pi$ state the fraction of ${}^2\Pi_{1/2}$ and ${}^2\Pi_{3/2}$ character is calculated, and then the formulas (2) and (3) are used. The parameters that follow from the best fit, which is also given in fig. 5, are: $\gamma_E = -3.15 \pm 0.20$ MHz, $\eta = (2.08 \pm 0.15) \times 10^{-3} \text{ cm}^{-1}$ and $\xi = (7.9 \pm 4.4) \times 10^{-3} \text{ cm}^{-1}$. The error is equal to one standard deviation. The physical origin of the two interaction parameters is such that the ratio ξ/η is equal to the ratio of the spin-orbit interaction constant A of the perturbing ${}^2\Pi$ state to the rotational constant B of the perturbed $E^2\Sigma^+$ state. Although the parameter ξ is not accurately determined we find a low value for the A constant, which is typical for the NO Rydberg states. This Rydberg state must mix with the $B^2\Pi$ non-Rydberg state causing the observed perturbation. Recently de Vivie [25] calculated the magnitude of the spin-orbit interaction between the $E^2\Sigma^+$ and the $B^2\Pi$ state for different values of the inter-

nuclear distance. The small value of about 1.0 cm^{-1} she finds for this interaction must be multiplied with the vibrational overlap before it can be compared with our value of ξ [23]. A typical vibrational overlap of 1% gives good agreement in sign and order of magnitude with the value of ξ we find.

It would be interesting to look for a similar perturbation in the $E^2\Sigma^+$, $v = 1$ state caused by the $B^2\Pi$, $v = 20$ state at rather low values of N , around $N = 9$ [23]. In the latter case the vibrational overlap will be larger and the perturbation will probably show up stronger.

5. Time evolution of the excited state populations

Time-resolved fluorescence both from the A state and the E state show directly the time evolution of the excited state populations. In fig. 7 the UV fluorescence from the $N = 1$ level in the $A^2\Sigma^+$, $v = 0$ state following pulsed laser excitation on the $A \leftarrow X Q_1(1)$ transition is shown. From this curve a radiative lifetime of $\tau = 208 \pm 7$ ns is found for the $N = 1$ level, in good agreement with literature values [18]. The relatively slow rise of the UV signal is somewhat peculiar; although the pulsed laser is on only for 10 ns, the maximum signal appears after 25 ns. This is due to a small retard-

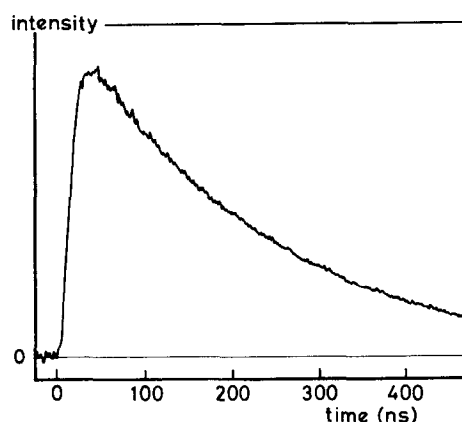


Fig. 7. Time-resolved A \rightarrow X fluorescence following pulsed laser excitation on the $A^2\Sigma^+$, $v' = 0 \leftarrow X^2\Pi$, $v'' = 0 Q_1(1)$ transition. A radiative lifetime of $\tau = 208 \pm 7$ ns is found for the $A^2\Sigma^+$, $v' = 0$, $N = 1$ level.

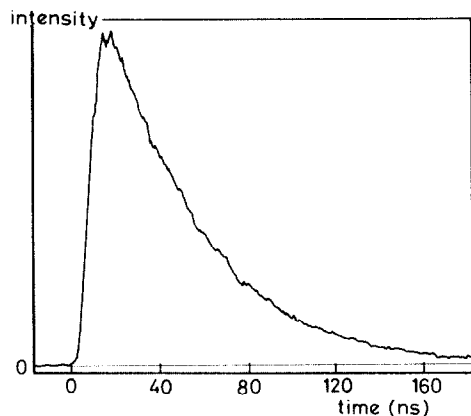


Fig. 8. Time-resolved E \rightarrow A fluorescence following pulsed laser excitation on the $E^2\Sigma^+, v=0 \leftarrow A^2\Sigma^+, v=0 P_1(1)$ transition. A radiative lifetime of $\tau = 41 \pm 2$ ns is found for the lowest rovibrational level in the $E^2\Sigma^+$ state.

ing effect of the PMT we used of about 12 ns; a pure exponentially decaying curve which starts instantaneously is changed into an exponential increasing curve minus the normal decay curve [26]. A similar retarding effect is of course also present in the other fluorescence curves and is taken into account in all simulations of the observed curves.

In order to determine the radiative lifetime of the E state we used two pulsed lasers in a similar double-resonance experiment. The NO($A^2\Sigma^+, v=0$) molecules are now excited to the $E^2\Sigma^+, v=0$ state using several mJ of red radiation from a Nd-YAG laser pumped pulsed dye laser operating on rhodamine B. The bandwidth of this laser was 0.5 cm^{-1} and the pulse length approximately 6 ns. With the pulsed UV laser on the $A \leftarrow X Q_1(1)$ transition and the second pulsed laser on the $E \leftarrow A P_1(1)$ transition the time-resolved E \rightarrow A fluorescence as shown in fig. 8 was obtained. The red laser was delayed by about 80 ns with respect to the UV laser. In this way a radiative lifetime of $\tau = 41 \pm 2$ ns is found for the $E^2\Sigma^+, v=0, N=0$ level. Within the experimental error the same lifetime was found for different N values up to $N=10$.

The lifetime of the E state can also be determined from the time-resolved pulsed-cw double-resonance E \rightarrow A fluorescence but, however,

less directly. As the cw laser connects both electronically excited states continuously the E-state fluorescence is not simply exponentially decaying. The population of the A state decreases exponentially in time. On the other hand, the excitation out of the A state will be more efficient for molecules that interact with the cw laser for a longer time. This suggests that the E-state fluorescence will be peaked at a somewhat later time, and that the exact shape of the fluorescence curve will depend on the applied cw laser power.

Once the radiative loss rates out of both excited electronic states are known, the time dependence of the E-state fluorescence in the pulsed-cw experiment can be quantitatively explained. The E state is continuously coupled to the A state by the cw laser. This coherent coupling lasts as long as there are molecules in the A state interacting with the cw laser, typically on a time scale of a few hundred ns. The coupling of the A state to the electronic ground state is only present for 10 ns, which justifies the description of the E-A system as an isolated two-level system. In this description we assume that at a given time zero a certain number of molecules are instantaneously pumped out of the ground state into the A state. At this moment there are no molecules in the E state yet. The two-level system described here is schematically given in fig. 9. It is an interesting and uncommon system in that both levels undergo radiative decay. The decay rates γ_1 and γ_2 are the inverse of the lifetimes of the A state and the E state respectively, and are set equal to $\gamma_1 = 4.80 \times 10^6 \text{ s}^{-1}$ and $\gamma_2 = 2.44 \times 10^7 \text{ s}^{-1}$. The rate of spontaneous fluorescence from the excited level in the E state back to the pumped level in the A state is indicated by γ_r . This parameter is not known precisely. All of the time-resolved E \rightarrow A state fluorescence measurements we discuss here are made with the cw laser set at the top of the Doppler-broadened profile of the single resolved $F' = 3/2 \leftarrow F'' = 5/2$ hyperfine component of the $E^2\Sigma^+, v'=0 \leftarrow A^2\Sigma^+, v''=0 P_1(1)$ transition (see fig. 4). For this special transition the rate γ_r is almost exactly 50% of the total E \rightarrow A emission rate, denoted γ_{21} [27]. It is known from VUV absorption and emission studies that only about 50% of the radiation absorbed in the E \leftarrow X tran-

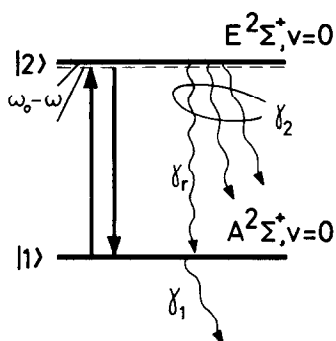


Fig. 9. Schematic representation of the two-level system described in the text. The total radiative loss rate out of the E state is equal to γ_2 and only a small fraction of this radiation (rate γ_r) radiates back into the initially pumped level in the A state. The radiative loss rate out of the A state is γ_1 . The solid arrows indicate the coherent (de)-excitation with the narrow-band cw laser, with a rate V .

sition is emitted to the ground state again [28]. On the other hand, the lifetime of the E state we measure is too long to make predissociation very probable. As the E \rightarrow A emission band is thought to be the strongest of the other radiative loss channels out of the E state [28], an E \rightarrow A fluorescence rate of $\gamma_{21} \approx \frac{1}{2}\gamma_2$ is deduced. The time evolution of such a two-level system can be correctly described using the Bloch equations for the compositions ρ_{11} , ρ_{22} , $\tilde{\rho}_{12} = \rho_{12} \exp(i \Delta\omega t)$ and $\tilde{\rho}_{21} = \rho_{21} \exp(-i \Delta\omega t)$ of the density matrix $\rho(t)$ as [29]:

$$\begin{aligned}\dot{\rho}_{11} &= \frac{1}{2}iV(\tilde{\rho}_{12} - \tilde{\rho}_{21}) + \gamma_r\rho_{22} - \gamma_1\rho_{11}, \\ \dot{\rho}_{22} &= -\frac{1}{2}iV(\tilde{\rho}_{12} - \tilde{\rho}_{21}) - \gamma_2\rho_{22}, \\ \dot{\tilde{\rho}}_{12} &= \frac{1}{2}iV(\rho_{11} - \rho_{22}) - \left(\frac{1}{2}\gamma_1 + \frac{1}{2}\gamma_2 - i\Delta\omega\right)\tilde{\rho}_{12}, \\ \dot{\tilde{\rho}}_{21} &= -\frac{1}{2}iV(\rho_{11} - \rho_{22}) - \left(\frac{1}{2}\gamma_1 + \frac{1}{2}\gamma_2 + i\Delta\omega\right)\tilde{\rho}_{21}.\end{aligned}\quad (4)$$

In these formulas V is the excitation rate [30], which is proportional to the square-root of the applied cw laser power, and $\Delta\omega = \omega - \omega_0$ is the detuning of the laser frequency ω with respect to the transition frequency ω_0 . The bandwidth of the cw laser (0.3 MHz) is much smaller than the natural linewidth of the NO E \leftarrow A transition (≈ 4.7 MHz). Therefore the laser profile is assumed to be infinitely narrow. The above system

of four coupled differential equations can be solved analytically if $\gamma_r = 0$ [29]. As pointed out above, in our case $\gamma_r \approx \frac{1}{4}\gamma_2$, of the same order as γ_1 , and certainly cannot be neglected. Therefore, we solved eqs. (4) numerically, with the initial conditions $\rho_{11}(0) = \rho_{11}(0, \Delta\omega)$, $\rho_{22}(0) = 0$, $\tilde{\rho}_{12}(0) = \tilde{\rho}_{21}(0) = 0$. The component $\rho_{22}(t)$ describes the time evolution of the E-state population, which is the quantity we determined experimentally.

Firstly, eqs. (4) will be used to fit the measured power dependence of the total (time integrated) E \rightarrow A state fluorescence. It will be shown that from such a fit the excitation rate V , which is in fact the only unknown parameter in our problem, can be accurately determined, for a given laser power. By taking the Laplace transform of the Bloch equations (4) it can be shown [29] that the total time-integrated E \rightarrow A fluorescence quantum yield, which is the quantity we measure with a large boxcar-gate, is proportional to:

$$\begin{aligned}\eta_2(\Delta\omega, V) &= \gamma_{21} \int_0^\infty \rho_{22}(t) dt \\ &= \frac{\gamma_{21}W}{\gamma_1\gamma_2 + W(\gamma_1 + \gamma_2 - \gamma_r)} \rho_{11}(0, \Delta\omega),\end{aligned}\quad (5)$$

with

$$W = \frac{V^2}{4} \frac{\gamma_1 + \gamma_2}{(\Delta\omega)^2 + [(\gamma_1 + \gamma_2)/2]^2}.\quad (6)$$

In our model the laser is assumed to be infinitely narrow, but the Doppler width can of course not be neglected. With the cw laser set on top of the Doppler broadened profile of a single resolved hyperfine transition the total fluorescence intensity we measure, I_{fl} , is proportional to:

$$\begin{aligned}I_{fl}(V) &\propto \int_{-\infty}^\infty \exp\left[-4 \ln 2(\Delta\omega/\Delta\omega_D)^2\right] \\ &\quad \times \eta_2(\Delta\omega, V) d\Delta\omega.\end{aligned}\quad (7)$$

The Doppler-width (fwhm) is set equal to $\Delta\omega_D = 2\pi \times 25$ MHz. For different values of the applied laser power, the intensity on top of the aforementioned hyperfine transition is measured, and the results are shown in fig. 10. In our setup the spatial variation of the applied cw laser power

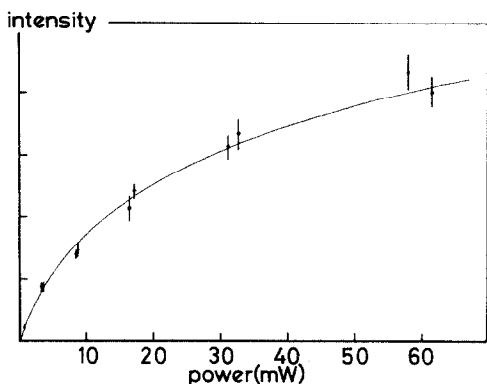


Fig. 10. Observed time-integrated E \rightarrow A fluorescence intensity as a function of the applied cw laser power. The cw laser is set at the maximum of the Doppler broadened profile of the single resolved $F' = 3/2 \leftarrow F'' = 5/2$ hyperfine component of the E \leftarrow A $P_1(1)$ transition (see fig. 4). From the best fit to the experimental points the relation between the excitation rate V and the applied laser power is determined.

can be neglected as only the central part of the Gaussian cw laser beam contributes to the observed double-resonance signal. This means that we can fit the observed points to the expression (7), taking a single value for V . From the best fit to the experimental points, which is also shown in the figure, we find

$$V = (4.7 \pm 0.3) \times 10^6 \text{ s}^{-1} \text{ at } 1 \text{ mW.}$$

The relation between the applied cw laser power and the excitation rate depends on the experimental setup. For our (special) setup the above relation holds, and can therefore be used later for the description of the observed time-resolved E \rightarrow A fluorescence. The reason why the excitation rate can be determined this precisely is that V appears in the formula (5) together with the known quantities γ_1 and γ_2 (γ_r is less important). A similar procedure is often followed to determine ionization rates in REMPI experiments where the lifetime of the intermediate state is known [31]. To determine the transition dipole moment for the E \leftarrow A transition from the relation between V and the applied cw laser power, only the photon flux (of the cw laser) needs to be known.

For the simulation of the observed E \rightarrow A fluorescence decay, the numerical solution of $\rho_{22}(t)$

from eq. (4) is needed. Again, the finite Doppler width has to be taken into account. This is done by adding the solutions for $\rho_{22}(t)$ for different values of $\Delta\omega$, i.e. by summing over different velocity groups. The number of molecules in each velocity group ($\rho_{11}(0, \Delta\omega)$) is weighted by a Gaussian envelope with a 25 MHz half-width. A typical time-resolved E \rightarrow A fluorescence decay curve is shown in fig. 11. This curve is an average over about 100 samples, with the cw laser set at the maximum of the line. A cw laser power of 58 mW (measured on the same relative scale as for the power dependence fit) was applied in this case, which yields a value of $V = 3.6 \times 10^7 \text{ s}^{-1}$ for the simulation. The simulation following eqs. (4) is given as curve I in fig. 11. The agreement between theory and experiment is excellent, especially when one considers that no parameters are fitted. Only the vertical scale of the calculated curve was adjusted. The slight deviations between theory and experiment can be explained by the approximations we made. The neglect of the spatial variation in the applied laser power is the most suspect assumption. In fact we should average over different curves, each for a slightly different value of V . A similar averaging is needed when we take into account the two different transition strengths of

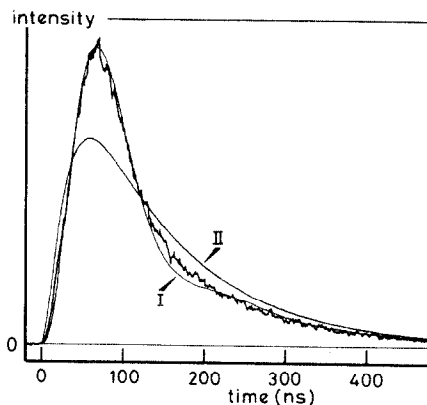


Fig. 11. Time-resolved E \rightarrow A fluorescence following excitation with the cw laser on the single resolved $F = 3/2 \leftarrow F = 5/2$ hyperfine component of the E \leftarrow A $P_1(1)$ transition. A cw laser power of 58 mW has been used. The simulation following the Bloch equations (curve I) as well as the experimental curve clearly show the effect of an oscillation around the solution following the master equation description (curve II) of the system.

the four possible M_F transitions; the transition dipole moment for the $|M_{F'}| = 1/2 \leftarrow |M_{F''}| = 1/2$ transition is about 20% larger than that for the $|M_{F'}| = 3/2 \leftarrow |M_{F''}| = 3/2$ transition. When both points are taken care of, the shallow dip around 160 ns in curve I can indeed be smeared out a little bit, although not completely. Because the spatial variation of the applied laser power (up to 20%) is not known and because trying two different transition strengths (with the same weighted average) hardly changes anything, we simplify by working with one value of V only. From the theoretical curve we deduce that in the peak, around 65 ns, as much as 17% of all the molecules initially in the probed hyperfine level of the $A^2\Sigma^+$ state have been excited to the $E^2\Sigma^+$ state by the cw laser. This seemingly low value is mainly due to the relatively large Doppler width; the velocity group that is exactly in resonance with the cw laser is almost 40% excited. This overall value of 17% is in good agreement with the magnitude of the fluorescence dips that, although weak, were observable in the total $A \rightarrow X$ UV fluorescence when the cw laser was scanned. Together with the PMT efficiency and the fluorescence quantum yields it also explains why the UV fluorescence is roughly a factor 100 more intense than the $E \rightarrow A$ double-resonance fluorescence, as seen in fig. 3.

Burshtein and Storozhev [29] have recently shown that, when $\gamma_r = 0$, the transition process has a typical "dephasing time" τ_{dp} given by $\tau_{dp} = 2/(\gamma_2 - \gamma_1)$. In our case this should mean that phase relaxation takes place on a time scale of 100 ns. Therefore, especially at short times, the quantum-mechanical description will be necessary. This is shown explicitly in fig. 11 by curve II which is the solution of the so-called balance or master equation treatment for the system. The master equations are obtained from the Bloch equations by setting $\dot{\rho}_{21} = \dot{\rho}_{12} = 0$ [29]. It is clear that the master equations will describe the situation correctly only when phase relaxation has taken place. The following set of master equations is found:

$$\begin{aligned} \dot{\rho}_{11} &= -(W + \gamma_1)\rho_{11} + (W + \gamma_r)\rho_{22}, \\ \dot{\rho}_{22} &= W\rho_{11} - (W + \gamma_2)\rho_{22}. \end{aligned} \quad (8)$$

The "classical" (non-coherent) excitation rate W , which is proportional to the applied laser power, is already given in eq. (6), as a function of the excitation rate V . An advantage of eqs. (8) is that an exact analytical solution can be given. Starting with the same initial conditions as before we find:

$$\rho_{22}(t) = \frac{W}{\lambda_+ - \lambda_-} (e^{\lambda_+ t} - e^{\lambda_- t}) \rho_{11}(0, \Delta\omega) \quad (9)$$

with

$$\begin{aligned} \lambda_{\pm} &= -[W + (\gamma_1 + \gamma_2)/2] \\ &\pm \left\{ [(\gamma_2 - \gamma_1)/2]^2 + W(W + \gamma_r) \right\}^{1/2}. \end{aligned} \quad (10)$$

It can easily be verified that the total time-integrated value of $\rho_{22}(t)$ from eq. (9) is exactly the same as that given by eq. (5). The master equation curve (curve II) is scaled relative to the Bloch equation curve (curve I), using eq. (6). Now a maximum excitation of nearly 12% is obtained. It is clear from fig. 11 that both the experimental curve and the exact theoretical curve (curve I) show the effect of Rabi oscillations, which cannot be explained with the master equations.

At lower laser powers the difference between both approaches becomes less evident. This is demonstrated in fig. 12, which is identical with fig. 11, but measured at roughly a factor 4 lower laser power (17 mW). The effect of the oscillations is less pronounced, although the description in terms

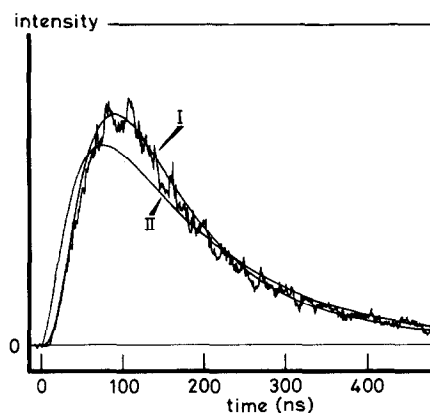


Fig. 12. Identical with fig. 11, but with 17 mW of cw laser power.

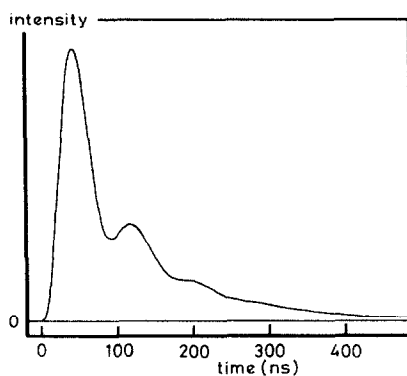


Fig. 13. Calculated time-dependent E \rightarrow A fluorescence when 250 mW of cw laser power is used. Only the correct solution, following out of the Bloch equations, is shown.

of the Bloch equations is still the only correct one. For short times the discrepancy between both approaches is still quite large.

At higher laser powers, on the other hand, strong oscillations are predicted. Although the finite Doppler width tends to smear out these oscillations, some additional maxima should be observable under the same experimental conditions, using only a slightly higher laser power. This is shown in fig. 13, which shows the calculated time dependence of the E \rightarrow A fluorescence when 250 mW of cw laser power is used ($V = 7.4 \times 10^6 \text{ s}^{-1}$).

6. Final remarks

It has been shown experimentally that the combination of a high-power pulsed laser with a narrow bandwidth cw laser makes a high-resolution study of highly excited electronic states possible. The signal-to-noise ratio on the double-resonance signal is shown to be very good. The use of a pulsed molecular beam and a more efficient detection scheme for the excited state population will provide further improvements. This suggests that this method has a very general applicability, also for the study of electronic states of less abundant transient species. From the time-resolved fluorescence curves the lifetimes of the excited states and the corresponding transition dipole moment can be determined. The observed Rabi oscillations

nicely demonstrate the coherence properties of a two-level system with radiative losses.

An experiment in which we tried to detect photoions formed by the cw laser was not successful. The main problem was that the photoions produced by the pulsed laser via (1 + 1)-REMPI caused a large ion background, which could not be completely discriminated against. For such an experiment it is advantageous to reduce both the linewidth and the energy per pulse of the pulsed laser, keeping the same spectral energy density. This gives less photoions, but the same A \leftarrow X excitation rate. Another possibility to distinguish between the different ion production channels, is in detecting photoelectrons. Only a very crude energy solution is needed for sufficient discrimination.

Another application of the present pulsed-cw double-resonance technique is in high-resolution studies of electronic states undergoing slow predissociation by which free atoms are formed. Even when the predissociation lifetime is as small as 0.1 ns a high-resolution study (e.g. resolution of hyperfine structure) is often still possible. From the spectral linewidths the quantum state dependent predissociation rates can then be accurately determined [32]. As the fluorescence quantum yield for these states is quite low, transitions to these states are difficult to be detected by normal LIF. In this case it is suggested to use a pulsed laser for the detection of the continuously formed photo-fragment atoms. The large bandwidth of the pulsed laser guarantees that all atoms, irrespective of their velocity, are detected. The same advantages as discussed before with regard to the detection efficiency as well as with regard to the reduction in background due to time resolved detection apply.

Acknowledgement

We wish to thank Dr. S. Stolte, Professors A. Dymanus and J. Reuss for helpful and stimulating discussions, and Professor D.H. Parker for a careful reading of the manuscript. The help of Drs. F. Keijzer in the experiment determining the lifetime of the E state using two pulsed lasers is gratefully

acknowledged. This work has been supported by the Stichting voor Fundamenteel Onderzoek der Materie (FOM) and has been made possible by financial support from the Nederlandse Organisatie voor Wetenschappelijk Onderzoek (NWO).

References

- [1] W. Demtröder, *Laser spectroscopy* (Springer, Berlin, 1982).
- [2] T.P. Softley, W.E. Ernst, L.M. Tashiro and R.N. Zare, *Chem. Phys.* 116 (1987) 299;
R.H. Page, R.J. Larkin, A.H. Kung, Y.R. Shen and Y.T. Lee, *Rev. Sci. Instr.* 58 (1987) 1616.
- [3] G. Meijer, J.J. ter Meulen, P. Andresen and A. Bath, *J. Chem. Phys.* 85 (1986) 6914.
- [4] G. Meijer, A.M. Wodtke, H. Voges, H. Schlüter and P. Andresen, *J. Chem. Phys.*, to be published.
- [5] D.H. Parker, in: *Ultrasensitive laser spectroscopy* (Academic Press, New York, 1983).
- [6] D.P. de Bruijn and J. Los, *Rev. Sci. Instr.* 53 (1982) 1020.
- [7] E. Riedle, R. Moder and H.J. Neusser, *Opt. Commun.* 43 (1982) 388;
P. Verkerk, D. Grand-Clement, F. Threhin and G. Grynberg, *Opt. Commun.* 58 (1986) 413.
- [8] K. Shimoda, ed., *Topics in applied physics*, Vol. 13. *High-resolution laser spectroscopy* (Springer, Berlin, 1976).
- [9] W. Ubachs, Ph. D. Thesis, Nijmegen, The Netherlands (1986);
G. Meijer, W. Ubachs, J.J. ter Meulen and A. Dymanus, *Chem. Phys. Letters* 139 (1987) 603.
- [10] A. Timmermann and R. Wallenstein, *Opt. Commun.* 39 (1981) 239.
- [11] E. Riedle, H.J. Neusser and E.W. Schlag, *J. Chem. Phys.* 75 (1981) 4231.
- [12] G. Meijer, M. Ebben and J.J. ter Meulen, *Chem. Phys. Letters* 147 (1988) 525.
- [13] E.E. Eyler, W.A. Chupka, S.D. Colson and D.T. Biernacki, *Chem. Phys. Letters* 119 (1985) 177.
- [14] C. Amiot and J. Verges, *Physica Scripta* 26 (1982) 422.
- [15] Chen Chuangtian, Wu Bochang, Jiang Aidong and You Guining, *Sc. Sinica B* 28 (1985) 235.
- [16] B.S. Hudson, *Spectroscopy* 2 (1987) 33.
- [17] S. Gerstenkorn and P. Luc, *Atlas du spectroscopie d'absorption de la moleculé d'iode* (CNRS, Paris, 1978); *Rev. Phys. App.* 14 (1979) 791.
- [18] L.G. Piper and L.M. Cowles, *J. Chem. Phys.* 85 (1986) 2419.
- [19] T. Bergeman and R.N. Zare, *J. Chem. Phys.* 61 (1974) 4500.
- [20] A. Lagerqvist and E. Miescher, *Helv. Phys. Acta* 31 (1958) 221.
- [21] H. Zacharias, private communication.
- [22] A. Lagerqvist and E. Miescher, *Can. J. Phys.* 44 (1966) 1525.
- [23] Ch. Jungen and E. Miescher, *Can. J. Phys.* 46 (1968) 987.
- [24] I. Kovacs, *Rotational structure in the spectra of diatomic molecules*, (Hilger, London, 1969).
- [25] R. de Vivie, Ph. D. Thesis, Bonn, FRG (1987).
- [26] *Manual R/P 065*, EMI Industrial Electronics LTD (1979).
- [27] R.W. Nicholls, *J. Res. Natl. Bur. Stds. A* 68 (1964) 535.
- [28] J.A. Guest and L.C. Lee, *J. Phys. B* 14 (1981) 3401.
- [29] A.I. Burshtein and A.V. Storozhev, *Chem. Phys.* 119 (1988) 1.
- [30] R. Loudon, *The quantum theory of light* (Clarendon Press, Oxford, 1985).
- [31] H. Rottke and H. Zacharias, *J. Chem. Phys.* 83 (1985) 4831.
- [32] W. Ubachs, J.J. ter Meulen and A. Dymanus, *Chem. Phys. Letters* 101 (1983) 1;
W. Ubachs, G. Meijer, J.J. ter Meulen and A. Dymanus, *J. Chem. Phys.* 84 (1986) 3032.
- [33] A.A. Radzig and B.M. Smirnov, *Reference data on atoms, molecules and ions* (Springer, Berlin, 1980).